!ARO 15848.6-EL

Contract DAAG29-78-C-0035

RESEARCH ON LONG WAVELENGTH BIAS-ASSISTED PHOTOEMITTERS

P. E. Gregory

Solid State Laboratory
Varian Associates, Inc.
611 Hansen Way
Palo Alto, CA 94303

1 October 1981

NOV 2 5 1981

Final Report for Period September 1978 through September 1981

Approved for public release; distribution unlimited.

81 11 24 070

| REPORT DOCUMENTATION PAGE | READ INSTRUCTIONS BEFORE COMPLETING FORM |
|---|---|

| 1. REPORT NUMBER | 2. GOVT ACCESSION NO. | 3. RECIPIENT'S CATALOG NUMBER |
|---|---|---|
| | AD-A112 815 | |

| 4. TITLE (and Subtitle) | 5. TYPE OF REPORT & PERIOD COVERED |
|---|---|
| Research on Long Wavelength Bias-Assisted Photoemitters | Final Report 25 Sept 78 -- 24 Sept 81 |
| | 6. PERFORMING ORG. REPORT NUMBER |

| 7. AUTHOR(s) | 8. CONTRACT OR GRANT NUMBER(s) |
|---|---|
| P. E. Gregory | DAAG29-78-C-0035 |

| 9. PERFORMING ORGANIZATION NAME AND ADDRESS | 10. PROGRAM ELEMENT. PROJECT. TASK AREA & WORK UNIT NUMBERS |
|---|---|
| Varian Associates, Inc. 611 Hansen Way Palo Alto, CA 94303 | |

| 11. CONTROLLING OFFICE NAME AND ADDRESS | 12. REPORT DATE |
|---|---|
| U.S. Army Research Office P. O. Box 12211 Research Triangle Park, NC 27709 | 1 October 1981 |
| | 13. NUMBER OF PAGES |
| | 40 |

| 14. MONITORING AGENCY NAME & ADDRESS(if different from Controlling Office) | 15. SECURITY CLASS. (of this report) |
|---|---|
| | Unclassified |
| | 15a. DECLASSIFICATION. DOWNGRADING SCHEDULE |

**16. DISTRIBUTION STATEMENT (of this Report)**

Approved for public release; distribution unlimited.

**17. DISTRIBUTION STATEMENT (of the abstract entered in Block 20, if different from Report)**

**19. KEY WORDS (Continue on reverse side if necessary and identify by block number)**

photocathode
infrared detector
InGaAs alloys

bias-assisted photocathode
field-assisted photocathode
MBE (molecular beam epitaxy)

**20. ABSTRACT (Continue on reverse side if necessary and identify by block number)**

The infrared threshold for photoemission has been extended to 2.1 $\mu$m by use of a bias-assisted lattice-mismatched $In_{.77}Ga_{.23}As/InAsP/InP$ photocathode. Quantum yield at 1.9 $\mu$m was $2 \times 10^{-3}$ electrons/incident photon, for 2.4V bias and a temperature of approximately 125K. This photocathode structure was grown by vapor phase epitaxy. Molecular beam epitaxy (MBE) has also been used to grow $In_{.77}Ga_{.23}As$/buffer/InP structures. The effect of different buffer layer

DD $_{1\ JAN\ 73}^{FORM}$ 1473 EDITION OF 1 NOV 65 IS OBSOLETE

schemes, including a superlattice structure, on MBE-grown $In_{.77}Ga_{.23}As$ mobility and photoluminescence was investigated.

Infrared imaging was demonstrated out to 1.65 $\mu m$ using an $In_{.53}Ga_{.47}As/InP$ bias-assisted photocathode operating in the transmission mode. Good reduction and sensitivity were obtained, indicating the potential usefulness of bias-assisted photocathodes for infrared imaging.

TABLE OF CONTENTS

# I.   INTRODUCTION

The long wavelength limit of useful sensitivity of conventional photocathodes is about 1.1 μm.  By conventional photocathodes, we mean all nonbiased photocathodes, e.g., S-1, alkali-antimonide and negative electron affinity photocathodes.  The development of externally-biased photocathodes has extended the infrared threshold to 2.1 μm.[1]  The general purpose of the work reported here is to improve the performance and understanding of this bias-assisted photocathode.

The infrared threshold of conventional photocathodes is due to a practical work-function minimum of about 1.0 eV at the electron-emitting surface.  Externally-biased photocathodes overcome this limitation by lowering the vacuum energy with respect to the bulk Fermi level by means of the applied bias.

Bias-assisted photoemission is based on the fact that for certain III-V semiconductors such as InP, GaAs, InGaAsP alloys and others,[2,3] electrons can be promoted to the upper conduction band valleys with reasonable efficiency for electric fields greater than $10^4$ V/cm.  Consider the energy band diagram of Fig. 1.  The cathode shown here is a low-bandgap (~0.9 eV) p-InGaAsP alloy on a p-InP substrate.  Photogeneration of minority carrier electrons can be achieved either by photons incident upon the electron emitting surface, the reflection mode of operation, R, or by photons incident upon the back substrate side, the transmission-mode of operation, T.  Photogenerated electrons quickly thermalize to the bottom of the Γ-conduction band minimum and a fraction begin to diffuse toward the emitting surface.  A reverse-biased Schottky-barrier surface contact depletes the p-InGaAsP cathode, establishing a field near the emitting surface of greater than $10^4$ V/cm.  The p-InGaAsP electron-emitting layer must be lightly p-type in order to achieve reasonably low internal Schottky-barrier leakage currents and at least several tenths of a micron of high electric field region needed for
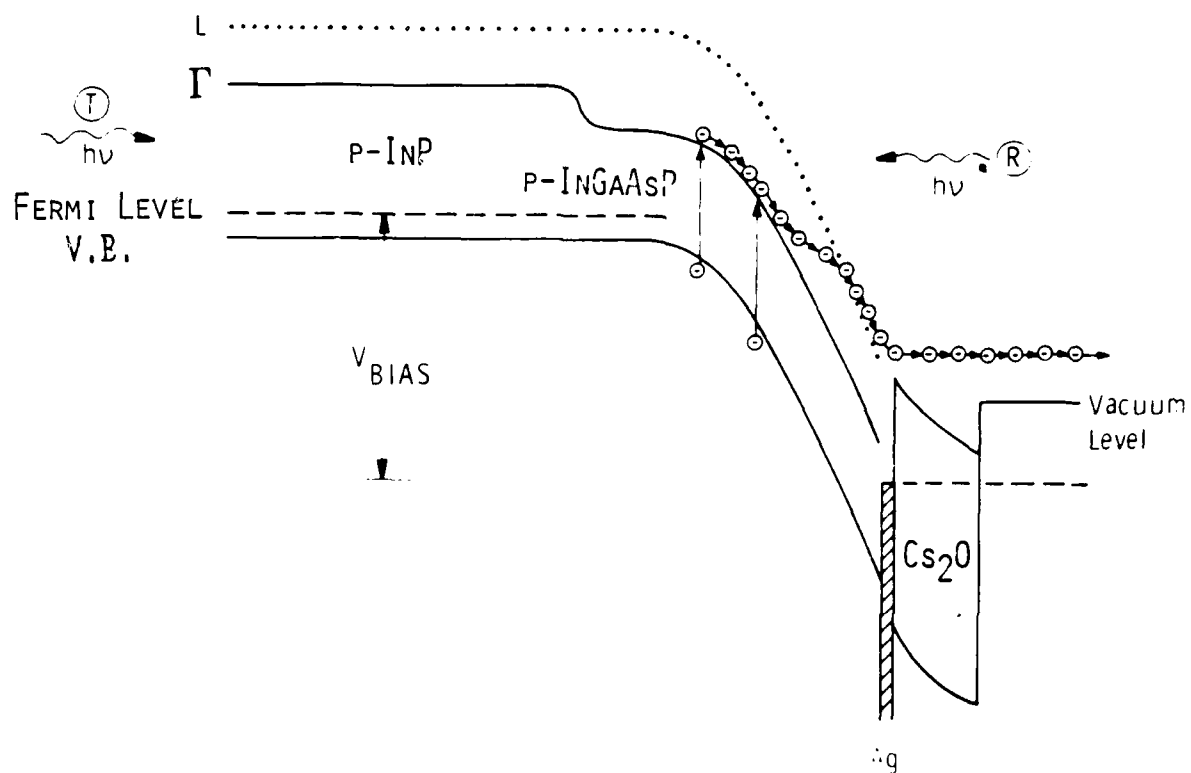
Fig. 1.    Energy band diagram of a Ag/p-InGaAsP
transferred-electron photocathode under bias
conditions.

2

efficient electron transfer. Electrons which successfully transfer to the upper conduction band valleys (e.g., L and X in the case of III-V alloys) or sufficiently hot $\Gamma$-electrons are then emitted over the surface energy barriers into vacuum. A low work function is attained by treatment of the Schottky-barrier metal and emitting surface with cesium and oxygen in a fashion similar to NEA activations.[4] A thin Ag film, ~150 Å thick, serves as an electron-permeable hole-barrier biasing contact.

Research on bias-assisted photocathodes has continued for over 20 years.[5,6] Many types of bias-assisted photocathodes, employing p-n junctions, MOS structures, Schottky barriers, field-emission, and hetero-junctions have been proposed and experimentally studied during this time. None of these photocathodes was successful in extending the threshold beyond 1.1 μm. In 1974, however, Bell et al.[7] experimentally demonstrated bias-assisted photoemission from an Ag/InP Schottky-barrier photocathode. The long-wavelength threshold was that of the InP band-gap, 0.92 μm (1.35 eV). Since 1974, work at Varian has steadily increased the long-wavelength threshold and increased the quantum efficiency of this type of bias-assisted photocathode.[8] Significant milestones in the development of the photocathode were the development of the Ag/InP/InGaAsP/InP heterojunction photocathode,[9] achievement of photoemission to 1.65 μm from As/InGaAsP/InGaAs/InP[10] and from Ag/InGaAs/InP,[11] achievement of 8% quantum efficiency at 1.55 μm,[8] the extension of the infrared threshold to 2.1 μm,[1] and the use of the bias-assisted photo-cathode for imaging.[12]

The bias-assisted photocathode work was supported by the Defense Advanced Research Projects Agency and the Night Vision and Electro-Optics Laboratory from January 1974 to February 1980,[13] and by the Army Research Office under an earlier contract[14] and under the contract covered by this report.

In the following sections, we discuss the work performed under this contract. The work includes the extension of the infrared threshold to 2.1 μm, growth of the bias-assisted cathode structure by molecular beam epitaxy (MBE), attempts to measure the energy distribution of electrons emitted from the photocathode, and the achievement of imaging from an ʌg/InGaAs/InP bias-assisted photocathode.

## II.    EXTENSION OF INFRARED THRESHOLD TO 2.1 μm

The infrared threshold for photoemission from a bias-assisted photocathode was extended to 2.1 μm by use of a lower-bandgap InGaAs alloy than had previously been used for bias-assisted photocathodes.

Figure 2 shows experimental reflection-mode yield curves for this photocathode for several bias voltages, measured at a temperature of ~125K.  For 2-V bias, the yield is above $1 \times 10^{-3}$ electrons per incident photon out to 1.94 μm.  Room-temperature yield measurements were also made, but no bias-assisted yield was found.  The room-temperature yield was similar to the zero-volt bias curve in Fig. 2 for up to 3-V bias.  A large improvement in long-wavelength yield upon cooling has also been seen for 1.65-μm InGaAs cathodes.[11]  The reason for this improvement with cooling is not known.

The photocathode energy band diagram is shown in Fig. 3.  The photocathode structure consists of p-InP substrate, a graded bandgap p-InGaAsP layer, a p-$In_{0.77}Ga_{0.23}As$ active layer, and a thin electron semitransparent silver Schottky barrier whose work function is lowered to ~1 eV with Cs and $O_2$.  The operation of this photocathode is similar to that described above in Sec. I.

The response of previous bias-assisted photocathodes[10,11,15] was limited to wavelength less than 1.65 μm by the 0.75-eV bandgap of the $In_{0.53}Ga_{0.47}As$ layer, which was grown directly on the InP substrate. $In_{0.53}Ga_{0.47}As$ has the smallest bandgap of the InGaAsP alloys that are lattice matched to InP.[16]  Thus for response beyond 1.65 μm, it is necessary to use an InGaAs composition which is not lattice matched to InP.  For good-quality epitaxial growth, it is necessary to provide a layer to grade between the InP and $In_{0.77}Ga_{0.23}As$ lattice constants. The InAsP layer serves this function.
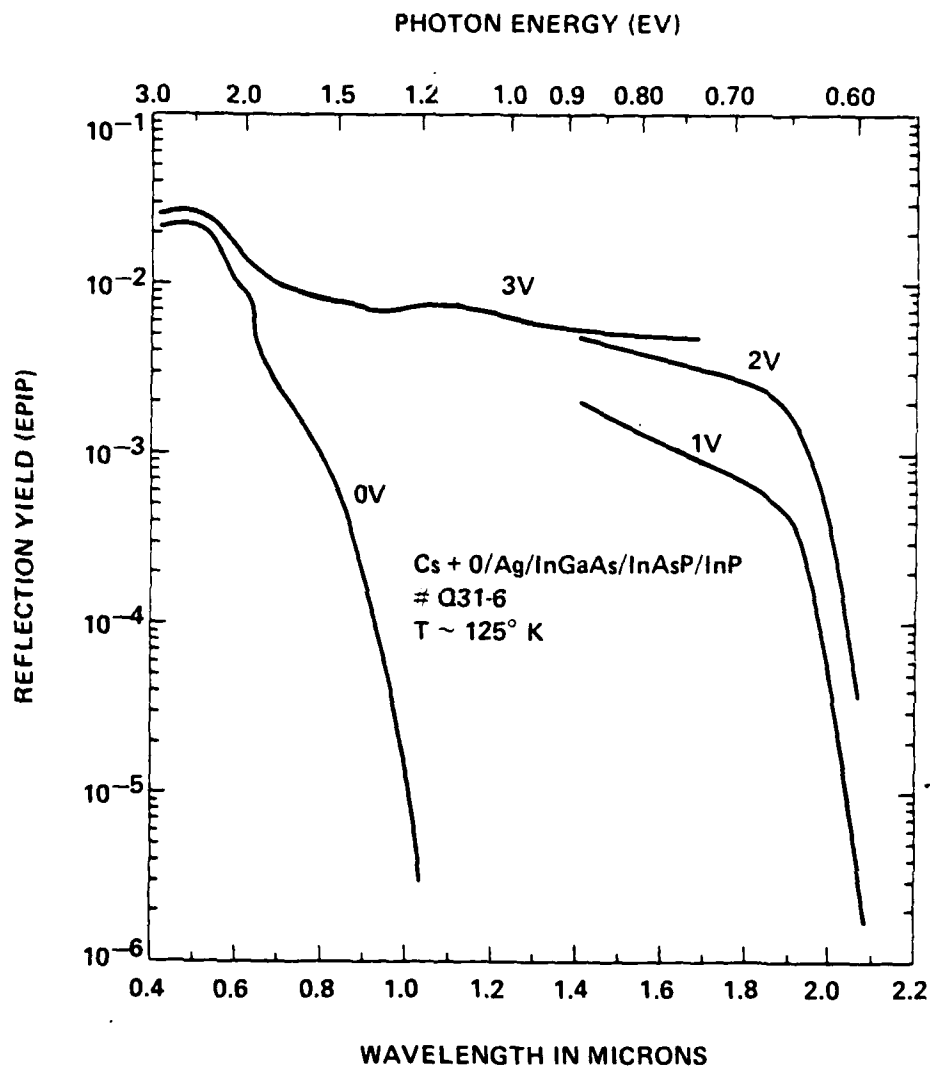
PHOTON ENERGY (EV)



Fig. 2    Experimental reflection-mode quantum yield curves for
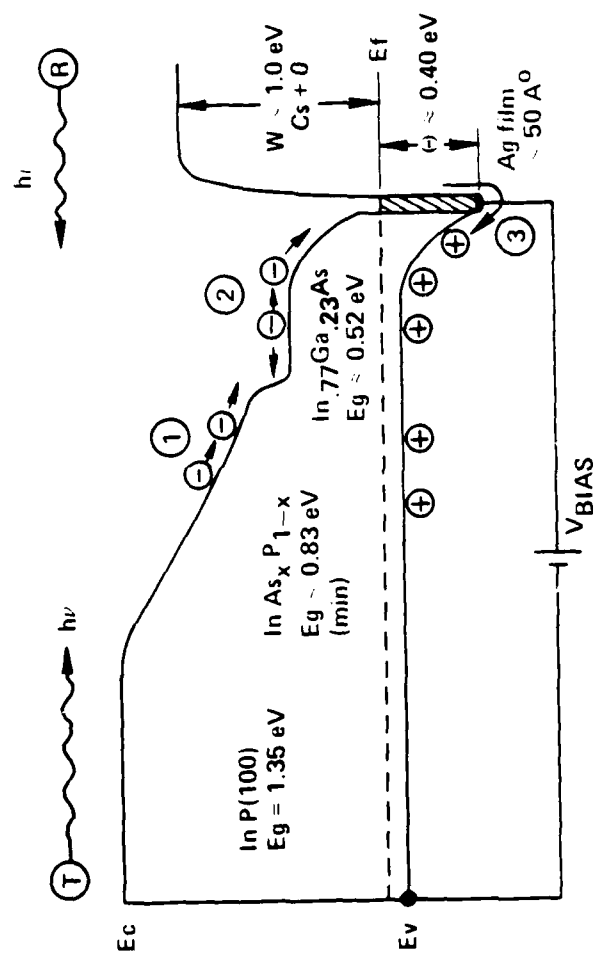          several bias voltages (noted above each curve).

6

Fig. 3   Energy band diagram for the photocathode.

7

The InAsP and $In_{0.77}Ga_{0.23}As$ layers were grown by vapor-phase epitaxy using the hydride process. The details of the growth procedures are described elsewhere.[17,18] Briefly, a mixture of 10% HCl in $H_2$ was passed over the In and/or Ga metal sources to form the metal chlorides which react with 10% $AsH_3$ in $H_2$ and/or 10% PH, in $H_2$ at the substrate to deposit the epitaxial layer. The compositional grading was done using a digital process programmer to control the inputs of the mass flow controllers.

The step-graded InAsP, doped p-type to about $10^{18}$ $cm^{-3}$, was grown on a Zn-doped InP (100) substrate. The grading in composition was accomplished by increasing the $AsH_3$ flow in steps of 0.5 cc/min, while the $PH_3$ and In-HCl flows were kept constant. The percent InAs change was about 2.2% per $AsH_3$ step up to $InAs_{0.22}P_{0.78}$ and about 1.4% from $InAs_{0.22}P_{0.78}$ to $InAs_{0.5}P_{0.5}$. A layer of $InAs_{0.51}P_{0.49}$ 1.5 μm thick was grown on the graded layer before depositing the lattice-matched $In_{0.77}Ga_{0.23}As$ layer. The InAsP layer was 15 μm thick, specularly reflective, and exhibited a cross-hatch pattern typical of compositionally graded layers.[18]

The $In_{0.77}Ga_{0.23}As$ was lattice matched to $InAs_{0.51}P_{0.49}$ by adjusting the In-HCl/Ga-HCl flow ratio. The $In_{0.77}Ga_{0.23}As$ was doped p-type to 5 x $10^{16} cm^{-3}$ and was 1.5 μm thick. The $In_{0.77}Ga_{0.23}As$ bandgap was ≈0.52 eV at 300 K as determined by photoluminescence at 77K.

After growth of the epitaxial layers, the photocathode was placed under ultrahigh vacuum and heated to remove surface oxides, and the Ag Schottky barrier film was evaporated. (The film was 6.1 x 2.5 $mm^2$ and ~50 Å thick.) Then the work function was lowered by exposure of Cs and $O_2$ until a peak white-light, nonbias-assisted yield was achieved.

Since the long-wavelength threshold is set by the InGaAs bandgap, it might be possible to extend the threshold to longer wavelengths than reported here, with the ultimate limit for this materials system of 3.54 μm (0.35 eV) for InAs. However, impact ionization may limit the threshold to shorter wavelengths than that. The threshold energy for impact ionization decreases with bandgap.[7,20] Thus for some bandgaps above that of InAs, the impact ionization may limit the electron energy to less than that needed to escape from the photocathode. More experiments will be needed to determine the ultimate long-wavelength threshold for this type of bias-assisted cathode.

In addition to extending the threshold further into the infrared, it should be possible to improve the quantum yield substantially. The doping of the InGaAs layer of the photocathode described above was not optimized. Further experimental work would be required to find the optimum doping level. Another modification of this photocathode which might improve its performance greatly is the addition of a lattice-matched InAsP emitter layer over the InGaAs layer. The InAsP emitter layer would have the same function as the InP emitter layer in the InP/InGaAs/InP heterojunction photocathode. The InP/InGaAs/InP photocathode has two advantages over the direct-emitting InGaAs/InP photocathode: it has higher quantum efficiency, and it is capable of room-temperature operation, whereas the direct-emitting photocathode requires cooling. The addition of an InAsP emitter layer to the 2.1-μm photocathode would probably result in the same improvements in performance.

One final area in which the 2.1-μm photocathode could be improved is in the quality of the lattice-mismatched InGaAs layer. Different lattice grading schemes might result in improved electrical properties in the InGaAs layer, and thus improve the photocathode performance. Several alternative lattice-grading schemes have been investigated, and are desscribed in the next section. However, more work would be required to assess the effect of the different grading schemes on actual photocathode performance.

## III. GROWTH OF InGaAs BY MBE

As discussed in the previous section, the infrared threshold for
bias-assisted photo emission was extended to 2.1 $\mu$m by use of a lattice-
mismatched $In_{0.77}Ga_{0.23}As$/graded-InAsP/InP structure, grown by chloride-
transport VPE. It has been proposed that the use of a superlattice
structure in place of the graded layer in a lattice-mismatched structure
will improve the electrical properties of the epitaxial layer grown over
the superlattice.[21-23] Molecular beam epitaxy (MBE) is capable of
growing semiconductor layers with thickness control down to single
monolayers, and has been very successfully used for superlattice growth.
Thus it was decided to investigate the growth of lattice-mismatched
InGaAs/buffer layer/InP structures by MBE to see if the InGaAs electrical
properties could be improved by the use of a superlattice buffer layer.

The aim of the work was to improve the performance of the 2.1-$\mu$m
bias-assisted photocathode by improving the InGaAs electrical properties.
The work described below did result in InGaAs with very good mobility
and photoluminescence efficiency. However, as will be discussed below,
an unexpected problem arose when growth was attempted on p-type InP
substrates. This problem prevented us from obtaining photoemission
results from the MBE InGaAs material.

The first step in developing MBE growth techniques for lattice-
mismatched InGaAs was to grow lattice-matched InGaAs on InP. The
$In_{.53}Ga_{.47}As$ was grown on InP using separate Ga and As cells. The
lateral uniformity measured by microprobe analysis showed practically no
variation ($\pm0.8$ atomic % within the detection limit of this technique),
in lattice constant across the 1.5-cm wafer. The solid composition of
InGaAs can be accurately predicted from the Ga/In flux ratio measured by
an ion gauge in the chamber before growth, enabling us to grow a lattice-
matched $In_{0.53}Ga_{0.47}As$ in the third attempt.

With the successful growth of lattice-matched InGaAs accomplished, the growth of lattice-mismatched $In_{0.77}Ga_{0.23}As$ was investigated. The effects of different buffer structures on the electrical and optical characteristics of these layers were compared to lattice-matched InGaAs layers. Figure 4 shows three different structures that were investigated. Figure 4(a) represents an $In_{0.77}Ga_{0.23}As$ layer grown directly on an InP substrate; Fig. 4(b) represents an $In_{0.77}Ga_{0.23}As$ layer grown on a graded buffer layer, and Fig. 4(c) represents an $In_{0.77}Ga_{0.23}As$ layer grown on a graded layer and an intervening superlattice.

The inclusion of a superlattice in the buffer structure was based on the work of Matthews and co-workers[21-23] on mechanisms of driving threading dislocations from vapor-phase epitaxial layers by glide under the influence of misfit strain. The technique involves repeated introduction of misfit strain greater than a certain threshold (to drive glide removal), between layers that are greater than a certain critical thickness determined by the misfit, but less than a thickness that would allow dislocation interaction and multiplication. This implies growth of a superlattice structure with minimum misfit between the layers for effective suppression of dislocation propagation in the growth direction. As already demonstrated, MBE is an excellent method of growing super-lattices.[24]

All the experiments were performed in a Varian MBE-360 system described previously.[25] For the growth of InGaAs, separate In and Ga effusion cells were used. For the superlattice structure, an additional In effusion cell was employed. A typical flux ratio of $As_4/Ga+In$ was 0.75. Before growth, the InP substrates were heat-cleaned in situ at 510°C for 5 minutes under As flux. A substrate temperature of 420°C was used for growth of $In_{0.53}Ga_{0.47}As$ or graded buffer layers. Superlattices and $In_{0.77}Ga_{0.23}As$ layers were grown at 380°C.

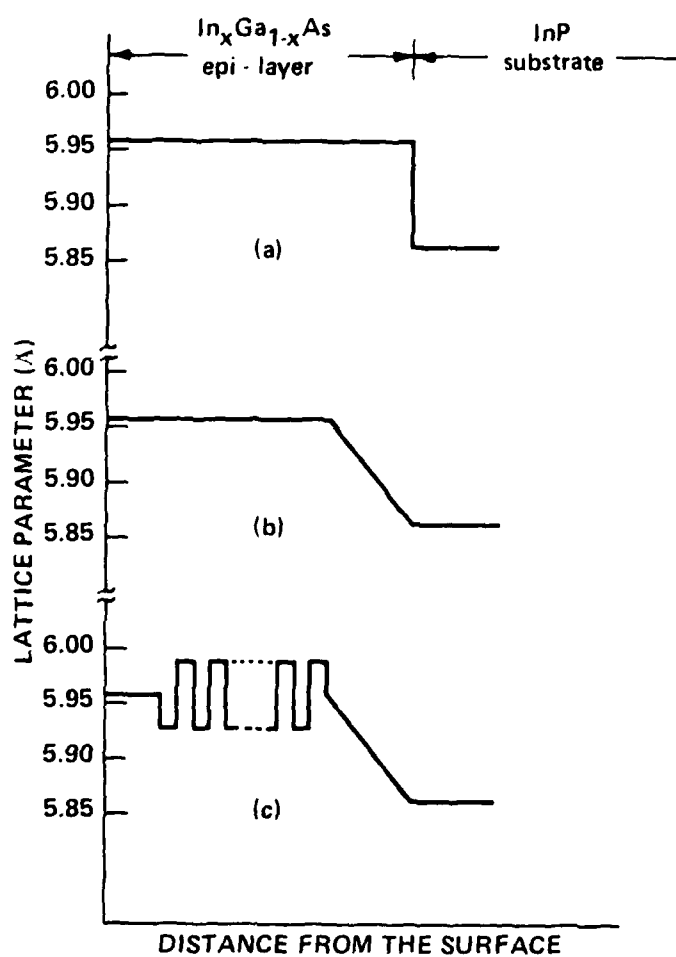Fig. 4    Three $In_{0.77}Ga_{0.23}As$ structures: (a) $In_{0.77}Ga_{0.23}As$ grown directly on an InP substrate, (b) $In_{0.77}Ga_{0.23}As$ grown on a graded layer, (c) $In_{0.77}Ga_{0.23}As$ grown on a buffer consisting of a graded layer and a superlattice.

Various analytical techniques were used to characterize the InGaAs layers: Nomarski high-contract microscopy was used for visual surface inspection, Hall mobility measurements were performed in a magnetic field of 1.1 KGauss, photoluminescence (PL) measurements at 77°K were made with an argon laser and a PbS detector, and etch pit counts were made. Initially, etch pit counts were made on surfaces etched in conventional AB etch used by Ettenberg, et al.[26] for characterizing InGaAs epilayers. However, this etchant was found to be too reactive with InGaAs layers, often dissolving the entire layer in 2-3 seconds; more reproducible results were obtained by dilution with 3 parts of HF.[27] The etch time was 2-3 seconds at room temperature.

As expected, the direct growth of lattice-mismatched $In_xGa_{1-x}As$ (x = 0.77) on an InP substrate resulted in different characteristics from those of lattice-matched InGaAs. Figure 5 shows surface pictures of typical layers, revealing the difference in the surface morphology. The lattice-matched InGaAs (Fig. 5(a)) had a smooth, shiny and featureless surface, whereas the surface of the lattice-mismatched InGaAs (Fig. 5(b)) had an orange-peel appearance. The usual Hall mobilities of the lattice-matched InGaAs were 7,000-8,000 $cm^2$/volt-sec at the room temperature with background carrier concentrations in the mid-$10^{15}cm^{-3}$. The mobilities of the $In_{0.77}Ga_{0.23}As$ ranged from 3,000 to 4,000 $cm^2$/volt-sec with background doping concentrations usually several times higher. The lattice-matched InGaAs showed a strong PL and the lattice-mismatched films had either weak or undetectable PL.

The etch pit count with diluted AB etchant turned out to be a rather inconclusive test of film quality. In Figs. 6(a) and (b), the etched surfaces of lattice-matched and -mismatched InGaAs on an InP substrate are shown for comparison. The etch pit configurations are different for the layers, i.e., well-defined circular boundaries on lattice-matched InGaAs and diffused boundaries on lattice-mismatched

13
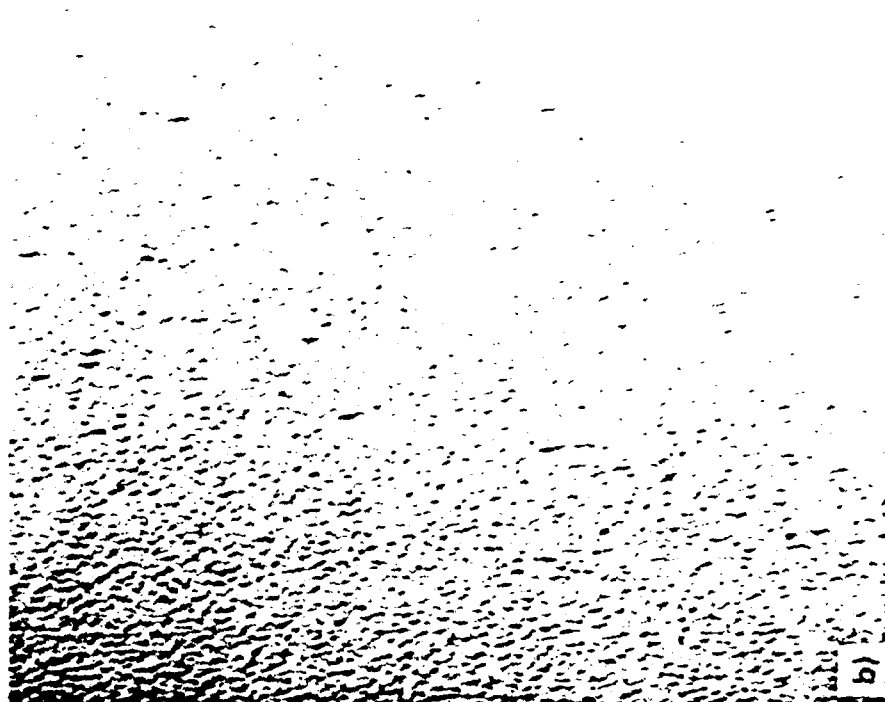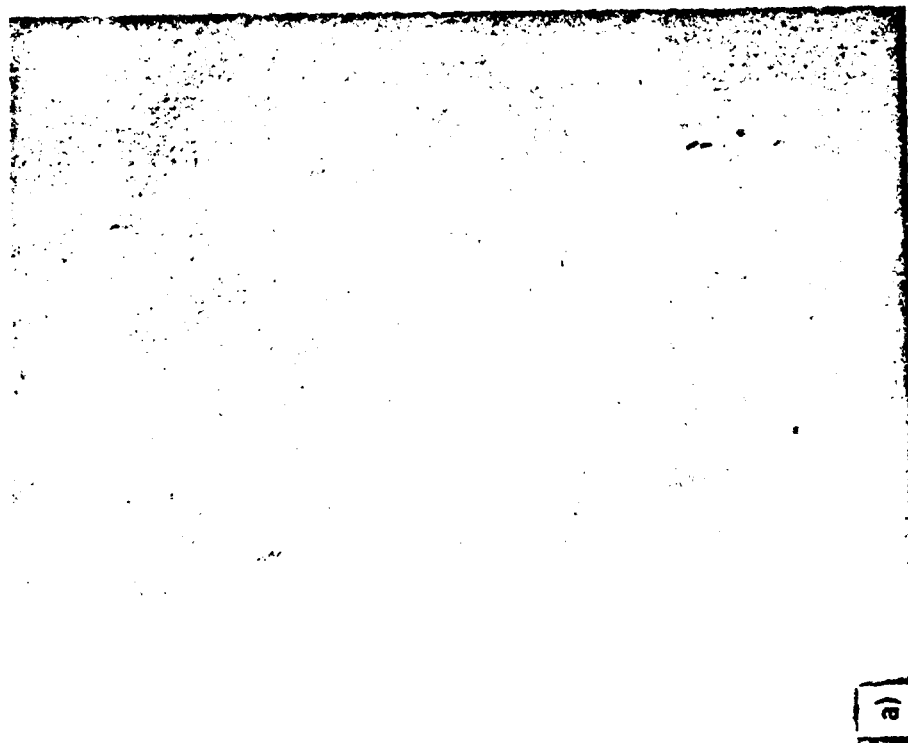
Fig. 5    Surfaces of: (a) the lattice-matched $In_xGa_{1-x}As$ (x = 0.53 and (b) the lattice-mismatched $In_xGa_{1-x}As$ (x = 0.77) grown directly on InP substrates.

50 μm

14
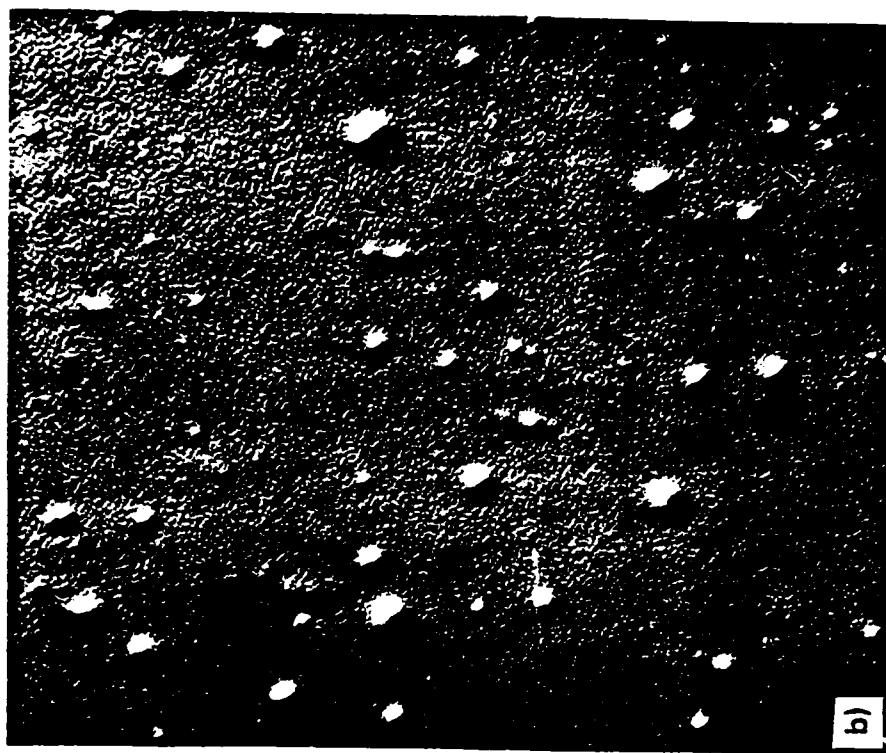
Fig. 6   Etch pits on:   (a) $In_{0.53}Ga_{0.47}As$ and $In_{0.77}Ga_{0.23}As$ as as revealed by 1 AB:3 HF.

$\vdash$ 100 $\mu$m $\dashv$

InGaAs. Also, the etch pit densities on the lattice-mismatched InGaAs were always <u>lower</u>, sometimes by an order of magnitude, than those on the lattice-matched InGaAs. The lower etch pit densities resulted in spite of severe lattice strain between the substrate and the epilayer, poorer electrical and weak photoluminescence characteristics of the lattice-mismatched InGaAs. It appears that this etchant does not reveal all the dislocations that affect the electrical and optical properties of the grown films.

The use of buffer structures, however, made significant improvements in the Hall mobilities and PL characteristics. Figure 7 shows the surfaces of three different buffer layers grown on InP substrates. Figure 7(a) represents a layer graded from $In_{0.53}Ga_{0.47}As$ to $In_{0.77}In_{0.23}As$. The grading rate was 24 atomic % of In over a thickness of about 0.6 μm. The next two photographs, Fig. 7(b) and Fig. 7(c) show superlattices grown on graded layers similar to Fig. 4(a). The superlattices in Fig. 7(b) consisted of 20 alternating layers of $In_{0.83}Ga_{0.17}As$ and $In_{0.70}Ga_{0.30}As$. Each layer thickness was 330 Å, making the total thickness of the super-lattice 0.66 μm. The superlattice in Fig. 7(c) consisted of 20 alternating layers of $In_{0.53}Ga_{0.47}As$ and InAs. Each layer thickness was about 130 Å. As shown in the photographs, all three layers had cross-hatched surfaces, but they are quite distinct from the surfaces of the lattice-matched $In_{0.53}Ga_{0.47}As$ or the lattice-mismatched $In_{0.77}Ga_{0.23}As$ grown directly on InP substrates as shown in Fig. 4. The higher density of cross-hatching on the superlattice of Fig. 7(c) compared to Fig. 7(b) is attributed to the larger mismatch between the superlattice and the $In_{0.77}Ga_{0.23}As$ lattice parameter, which are ±1.3% and ±0.5%, respectively.

The superlattice with the higher density cross-hatches also had a higher etch pit density. Figure 8 shows the etch pits on the buffers shown in Fig. 7. The etch pit densities on the superlattice with higher lattice strain (Fig. 8(c)) showed etch pit densities several times higher than those on the superlattice with less lattice strain (Fig.

16
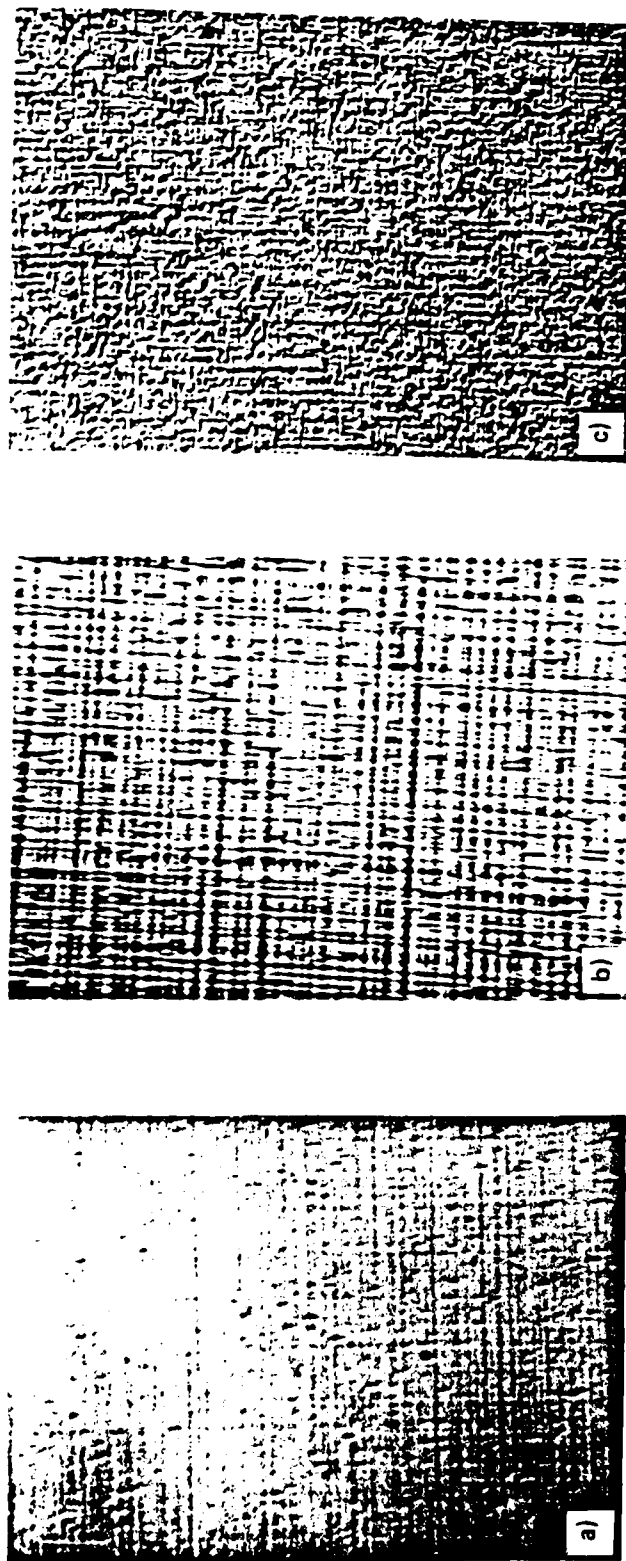
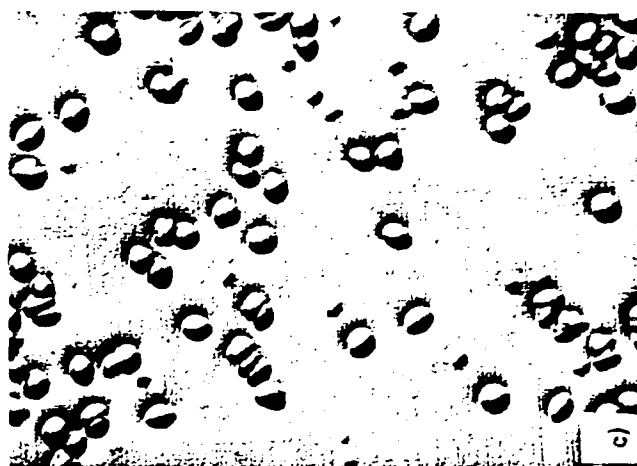Fig. 7   Surfaces of:   (a) a graded buffer, (b) $In_{0.70}Ga_{0.30}As/In_{0.84}Ga_{0.16}As$ superlattice grown on a graded layer, and (c) the $InAs/In_{0.53}Ga_{0.47}As$ superlattice grown on a graded layer.
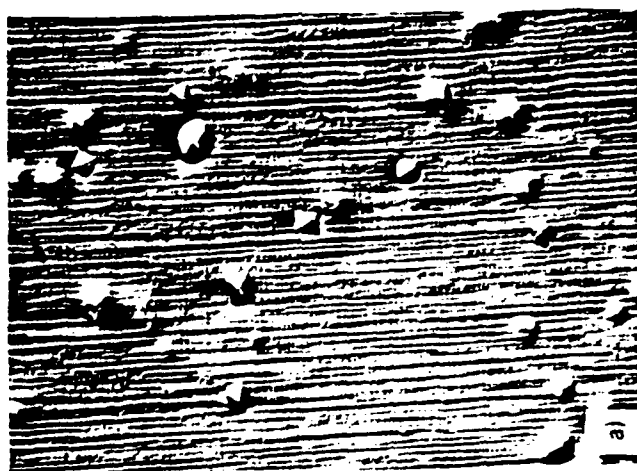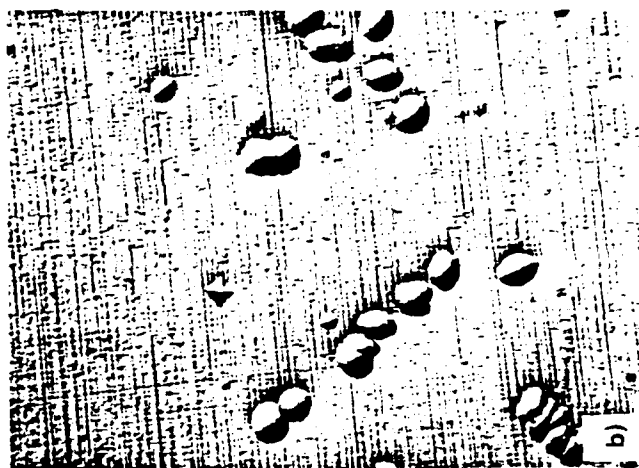
50 μm

Fig. 8    Etch pits on the buffer surfaces of Fig. 4.

100 μm

18

8(b)). It also may be noted that the etch pits on the graded buffer in Fig. 8(a) had a different shape than those of the superlattice buffers. They look more like the etch pits on $In_{0.77}Ga_{0.23}As$ films directly grown in InP substrates. Sometimes the etch pits are rectangular shapes, as shown in the figure. When the etch pit densities were compared between the graded buffer (Fig. 8(a)) and the superlattice buffers (Figs. 8(b) and (c)), the etch pit density on the graded buffer was several times lower than those on the superlattice buffer, even though the difference is not obvious from the pictures shown in Figs. 8(a), (b), and (c).

Figures 9(a) and (b) show the surface of 1.8-μm thick layers of $In_{0.77}Ga_{0.23}As$ grown on the buffers shown in Figs. 8(a) and (b). These layers have improved electrical and optical characteristics over the layers directly grown on InP substrates. The greatest improvement occurred in the PL characteristic shown in Fig. 10. Figure 10(a) represents the PL from a layer grown directly on an InP substrate. The PL intensity was so low that it cannot be seen in this scale. Figures 10(b) and (c) represent the PL from layers grown on a graded buffer (b) and on a buffer consisting of a graded layer plus ±0.5% mismatched superlattice (c). The improvement is dramatic. For comparison, the PL from a lattice-matched InGaAs is shown on the left hand side of the figure on the same scale. Despite the higher etch pit densities on the buffer, the PL intensity from the layer grown on the superlattice buffer (c) is twice as high as the PL from the layer grown on a graded buffer (b), again calling into question the validity of using AB etch pit counts as a measure of film quality. For fair comparison, all these layers were grown about the same time, within a one-week interval, and the PL measurements were made on the same day. As shown in Fig. 10, the PL from the film grown on the superlattice buffer is about 2/3 of that from the lattice-matched InGaAs, indicating high quality of the lattice-mismatched film grown on this buffer.
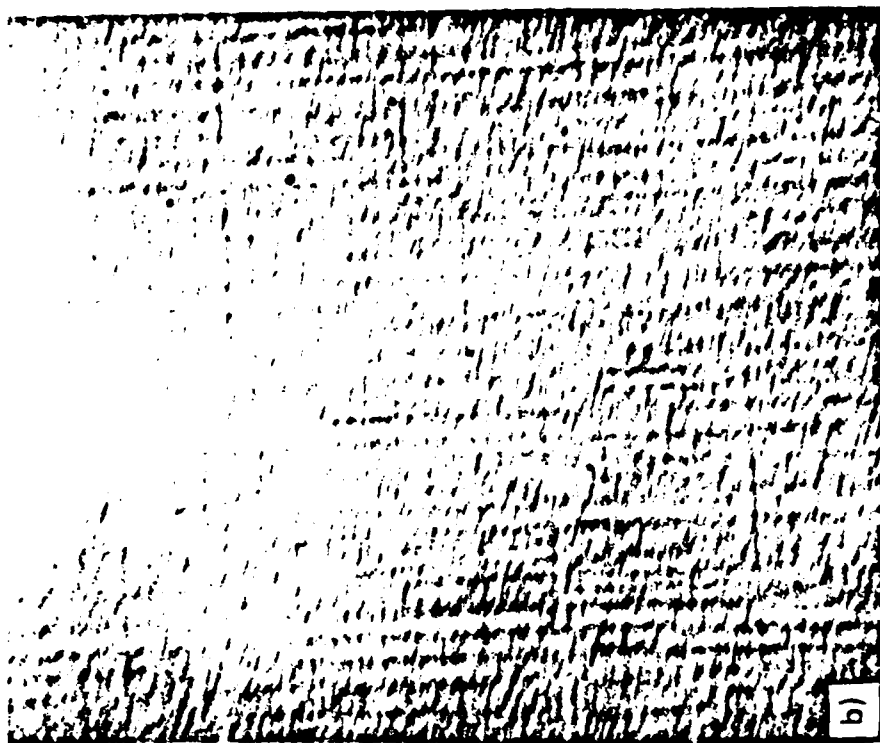
Fig. 9   Surfaces of 1.8-µm thick $In_{0.77}Ga_{0.23}As$ grown on (a) a graded buffer and (b) $In_{0.70}Ga_{0.30}As/In_{0.84}Ga_{0.16}As$ superlattice grown on a graded layer.
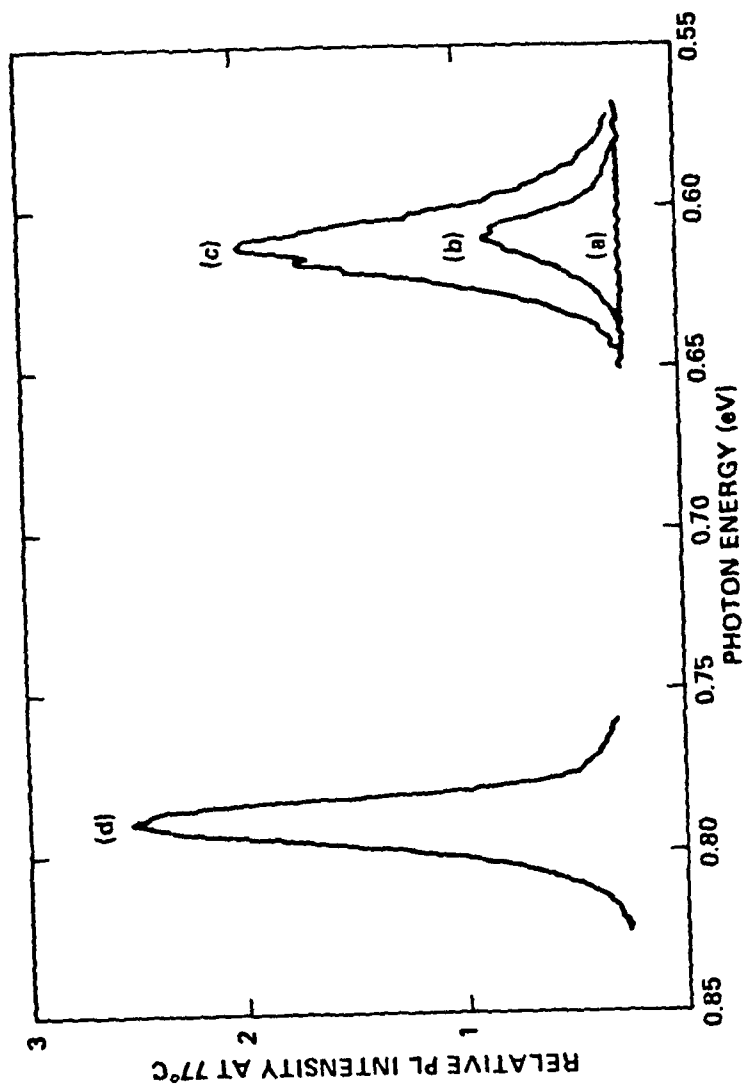
50 µm

Fig. 10  77°K PL intensities from $In_{0.77}Ga_{0.23}As$ layers; the layer (a) grown directly on an InP substrate, (b) grown on a graded buffer, and (c) grown on the $In_{0.70}Ga_{0.30}As/In_{0.84}Ga_{0.16}As$ superlattice. For comparison, the PL intensity from a lattice-matched InGaAs is shown on the left at the same scale.

There was also substantial improvement in the Hall mobilities. Table I shows the results, along with the other data. For comparison, the properties of $In_{0.53}Ga_{0.47}As$ and the $In_{0.77}Ga_{0.23}As$ directly grown on InP substrates are also given. As can be seen, the room-temperature Hall mobilities of $In_{0.77}Ga_{0.23}As$ grown on buffers are about twice the mobility of the $In_{0.77}Ga_{0.23}As$ directly grown on InP substrates. These mobilities of the lattice-mismatched InGaAs grown on buffers are as good as or better than that of lattice-matched InGaAs. The unintentional background doping concentrations for the $In_{0.77}Ga_{0.23}As$ are higher than those for the lattice-matched InGaAs, by more than an order of magnitude. The PL intensities at liquid nitrogen temperature (see Table I) also show a dramatic increase in intensity for the $In_{0.77}Ga_{0.23}As$ layers grown on buffers over a similar layer grown directly on the InP substrate. In spite of the improvement of the layer quality, however, etch pit densities do not reflect this improvement. In fact, $In_{0.77}Ga_{0.23}As$ grown directly on InP shows the lowest etch pit density, despite its low Hall mobilities and poor PL characteristics.

To summarize the MBE growth results, lattice-mismatched $In_xGa_{1-x}As$ (x = 0.77) on InP substrates by MBE with good electrical and optical characteristics were obtained. This was accomplished by using a buffer, either a graded layer or a buffer consisting of a graded layer plus superlattice. The use of the buffer resulted in Hall mobilities of almost 8,000 $cm^2$/volt-sec and PL intensities at 77°K, comparable to the lattice-matched $In_xGa_{1-x}As$ (x = 0.53). A comparable mobility was obtained using a graded layer without a superlattice. However, the addition of a superlattice layer at the end of the graded layer seemed to improve the PL intensities of the final $In_{0.77}Ga_{0.23}As$ layer. We also found that etch pits revealed by the AB etch was not a good indicator of layer quality, since they correlated poorly with the improvement reflected in the electrical and optical characteristics of the layers. It appears that the AB etch does not reveal all the dislocations on the low-bandgap $In_xGa_{1-x}As$.

22

TABLE I: Properties of MBE-grown $In_{0.53}Ga_{0.47}As$ and $In_{0.77}Ga_{0.23}As$

| WAFER NUMBER | EPILAYER | MEASURED CARRIER CONCENTRATION ($CM^{-3}$) | HALL MOBILITIES AT RT ($cm^2/V$-sec) | ETCH PIT ($cm^{-2}$) | RELATIVE PEAK PL INTENSITY |
|---|---|---|---|---|---|
| IGA 86 | Lattice-Matched InGaAs on an InP Substrate | $7.6 \times 10^{15}$ | 7,200 | $8.1 \times 10^4$ | 320 |
| IGA 91 | $In_{0.77}Ga_{0.23}As$ on an InP substrate | $1.2 \times 10^{17}$ | 3,900 | $7.4 \times 10^3$ | 3 |
| IGA 95 | $In_{0.77}Ga_{0.23}As$ on a Graded Buffer | $6.6 \times 10^{16}$ | 7,900 | $1.9 \times 10^4$ | 100 |
| IGA 93 | $In_{0.77}Ga_{0.23}As$ on a Graded Buffer Plus Superlattice | $3.8 \times 10^{16}$ | 7,050 | $1.6 \times 10^5$ | 200 |

An attempt was made to grow InGaAs layers for use as field-assisted photocathodes, but an unexpected problem arose. All of the work described above, and previous lattice-matched InGaAs growth studies were done on Fe-doped semi-insulating InP substrates. It is necessary to have a conducting substrate (preferably p-type) for field-assisted photocathodes. When $In_{0.53}Ga_{0.47}As$ was grown on a p-type substrate, it was found to produce very little or no PL response. Several experiments were conducted in an attempt to overcome, or at least understand, this problem. InGaAs was grown on Fe-doped and p-type InP substrates simultaneously mounted side by side on the same heater block. The result was the same; good PL intensity from the layer on the Fe-doped substrate, but none detectable from the layer on the p-type substrate. A continuous outgassing of the In and Ga charges overnight in the MBE system increased the PL signal strength from layers on Fe-doped substrates, and produced a detectable PL signal from layers on p-type substrates. However, the PL from the layer on the p-type substrate was still much lower than that from the layer on the Fe-doped substrate. We do not yet understand the origin of the difference in quality of the InGaAs grown on the two types of substrates. P-type substrate material from the same boule has been used successfully for other projects in this laboratory, so it is of good quality. Perhaps there is some interaction between the Be dopant in the InGaAs layer and Zn from the substrates.

An attempt was made to fabricate a field-assisted photocathode from an InGaAs on p-InP sample. This sample was one of the earlier growths, made before it was found that the PL strength could be improved by outgassing the In and Ga sources. The photocathode did not exhibit any field-assisted photoemission at room temperature or at ~125°K. This result is not surprising in view of the low PL intensity from the InGaAs layer of this sample.

The MBE-grown InGaAs results are very encouraging, notwithstanding the difficulties encountered in growth on p-type InP. The mobility

achieved for $In_{0.53}Ga_{0.47}As$ (7200 $cm^2$/V-sec of room temperature) is comparable to or better than that obtained by LPE[28] and VPE.[29] This high mobility was also obtained for lattice-mismatched InP grown on graded buffer layers and graded buffer layers plus superlattices. Thus InGaAs layers of device quality can now be grown by MBE over a range of bandgaps, as long as p-type substrates are not required. If the problem in growing on p-type InP can be overcome, the MBE material shows great promise for use as field-assisted photocathodes with response out to 2 µm.

IV.   MEASUREMENT OF ELECTRON ENERGY DISTRIBUTIONS

An attempt was made to measure the energy distribution curve (EDC) of electrons emitted from a bias-assisted photocathode. There were two reasons for wanting to know the energy distribution of emitted electrons. First, it is useful to know the energy spread of the emitted electrons to assess the possible performance of the bias-assisted photocathode in actual tube structures. In particular, it was feared that the emitted electrons would have such a large energy spread as to make it very difficult to focus them for imaging applications. Secondly, Monte Carlo hot electron transport calculations for the bias-assisted InP photocathode had given internal electron energy distributions,[30] and it was desired to compare the theoretical internal energy distributions to measured emitted electron energy distributions.

Equipment to measure EDCs was set up in one of the photocathode activation vacuum systems. EDCs were measured using the standard retarding potential technique.[31] The electron energy analyzer was a standard Varian 4-grid LEED analyzer with the electron gun removed. Light from the monochromator passed through the holes normally used for the electron gun, and struck the photocathode at normal incidence. A bias plate was placed between the photocathode and the analyzer in order to apply bias to the photocathode Schottky barrier, while keeping stray electrical fields out of the energy analyzer. A 0.18" x 0.06" hole in the bias plate allowed the incident light to reach the photocathode. Contact to the photocathode Schottky barrier was made by a raised lip 0.015" high around the hole in the bias plate. The bias plate was grounded and negative bias applied to the photocathode.

EDCs were measured both from bias-assisted InP and NEA GaAs photocathodes. The results were not satisfactory, however. It was found that for both bias-assisted and NEA photocathodes, at least -3 volts bias was required on the photocathode to get electrons into the energy

analyzer. This behavior was probably caused by a retarding field caused by the difference in work function between the bias plate and the cesiated photocathode surface. Similar effects have been reported in the literature.[32,33]

A more important problem was the fact that the EDCs were not completely reproducible. Some EDCs were considerably broader than others. In some cases, the broadening could be attributed to degraded energy analyzer resolution caused by variations in the work function within the energy analyzer due to uneven cesium deposition. In other cases, however, the shape of the EDC varied depending on where the bias plate touched the silver Schottky barrier. This effect may have been caused by uneven cesiation of the silver film, or by variations in the film thickness.

The difficulties described made it evident that much more work would be required before meaningful EDCs could be measured from bias-assisted photocathodes. However, the imaging experiments, described in the next section, answered the most important question regarding the electron energy. They demonstrated that images with acceptable resolution can be produced by a bias-assisted photocathode, using only proximity focusing. The electron energy spread has no apparent adverse effect on the image. Therefore, it was decided not to pursue the EDC experiments further.
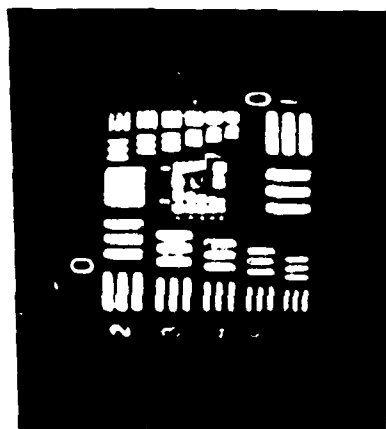
V.    IMAGING FROM AN As/In$_{0.53}$Ga$_{0.47}$As/InP BIAS-ASSISTED PHOTOCATHODE

In order to test the suitability of the bias-assisted photocathode
for imaging applications, an in-situ imaging apparatus was added to one
of the photocathode activation vacuum systems.  Images were projected
onto the back of a bias-assisted photocathode operating in the semi-
transparent mode.  Electrons emitted from the front cf the photocathode
are proximity-focused onto a phosphor screen which is attached to a 2X
fiber-optic image expander.  The resulting image is viewed and photo-
graphed through a vacuum window.  The imaging apparatus was developed
under support of NVL contract DAAK02-74-C-0132.  The imaging work under
that contract concentrated on the Ag/InP/InGaAs/InP photocathode, and
has been reported elsewhere.[12,13]  Here we report imaging results of a
direct emitter, Ag/InGaAs/InP bias-assisted photocathode.

Figure 11 shows images of the Air Force 1951 resolution pattern
made with 1.61 μm and 1.12 μm light.  Resolution tests showed that 20-22
line pairs per mm could be resolved by the photocathode.  (The resolu-
tion cannot be directly read from the photographs because the test
pattern was not projected onto the photocathode at a 1:1 ratio.)  The
active area of the photocathode was approximately 1/3 inch in diameter.

Figure 12 shows views of a parking lot outside the laboratory, pro-
jected onto the photocathode with a lens and a mirror.  The detail in
the photographs of Fig. 12 shows that the bias-assisted photocathode can
produce high-quality images.  The images in Fig. 12 were made in day-
light, but limited to the 0.9-1.65 μm spectral region by the bandgaps of
the InP and InGaAs layers of the photocathode operating in the semi-
transparent mode.  The lens used to project the images on the photo-
cathode was designed for use in the visible region, and is probably not
well suited for the 0.9-1.65 μm spectral region.  The white dots outside
the image area were caused by field emission from flaws in the phosphor

1.61 micron light
2.0V bias, -130°C
Ag/p-InGaAs/InP
0.83 cm dia. Ag,
1/2" dia. cathode
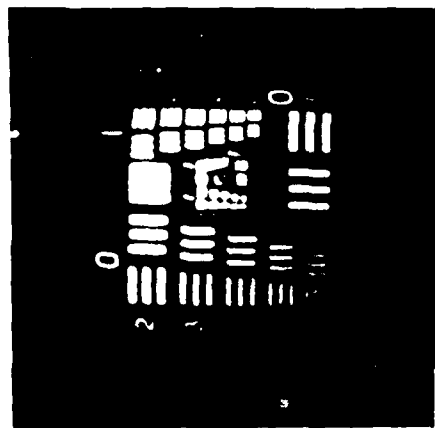
1.12 micron light
In-Situ imaging
14.2" f.l. lens,
aprox. 20-221pm
limiting resol.

Fig. 11 Test pattern images made by a direct emitter, $Ag/In_{0.53}Ga_{0.47}As/InP$ bias-assisted photocathode.

cars in bright
sun

car viewed
through trees

foliage on
fence

cars in bright
sun

truck tire

Fig. 12  Daytime photos of cars and foliage in
parking lot using light in 0.9-1.65 μm
spectral range.  Cars are at ~100 yards
distance, lens used has 14.2-inch focal
length.  Photocathode used was
$Ag/In_{0.53}Ga_{0.47}As/InP$, number PC-85,
under 2V bias and cooled to -130°C.

screen. The bright cresent-shaped area in the lower right portion of the images is also an artifact caused by a flaw in the phosphor screen.

The ability of a bias-assisted photocathode to form an image under low light levels was demonstrated in another measurement.[13] Using an Ag/InP/InGaAs/InP photocathode, it was possible to form an image with 1.5-$\mu$m light with intensity as low as $1.1 \times 10^{-9}$ watts/cm$^2$ ($8.3 \times 10^9$ photons/sec-cm$^2$). Since there was no microchannel plate in the imager, gain was achieved by photographing the phosphor screen using long exposures (as long as 2 hours).

The imaging results are quite important, since the major application for the bias-assisted photocathode was to be for night vision devices. The fact that high-quality images can be produced with the bias-assisted photocathode also demonstrates that the energy spread of the emitted electrons is not so large as to interfere with focusing of the electron image.

# VI.    CONCLUSIONS AND RECOMMENDATIONS

Very encouraging progress has been made in the development of bias-assisted photoemitters under this contract.  The two most significant results were the extension of the infrared threshold to 2.1 µm and the demonstration of high-quality imaging out to 1.65 µm using a bias-assisted photoemitter.

There are two broad areas where more work is needed in the development of the bias-assisted photocathode:  development work on the 1.65-µm InP/In$_{0.53}$Ga$_{0.47}$As/InP photocathode, and further work on extending the infrared threshold and improving the quantum efficiency of the 2.1-µm bias-assisted photocathode.  The 1.65-µm photocathode is already well-developed, having demonstrated high quantum efficiency and the ability to operate in a semi-transparent imaging mode.  There are, however, still several areas in which work is needed if it is ever to be used for night vision applications.  They are:  operation with a microchannel plate to assess its usefulness under very low light level conditions, optimization of the dark current performance of the photocathode, and testing of a sealed-off image tube under realistic field conditions to assess the usefulness of the bias-assisted photocathode as a night vision device.

There is much more work to be done in developing the 2.1-µm photocathode.  As discussed in Section II, the ultimate infrared threshold for this device may be beyond 2.1 µm; more work is required to find how far the threshold may be extended.  There is also reason be believe that the quantum efficiency of this device can be greatly improved.  The MBE work on In$_{0.77}$Ga$_{0.23}$As growth shows that the electrical properties of the material can be improved by the use of a superlattice matching layer.  Furthermore, the use of a lattice-matched InAsP emitter layer over the In$_{0.77}$Ga$_{0.23}$As absorber layer would probably improve the quantum efficiency and allow the photocathode to operate with less cooling than was required for the structure described in Section II.

## VII.    REFERENCES

1.  P. E. Gregory, J. S. Escher, R. R. Saxena and S. B. Hyder, Appl. Phys. Lett. 36, 639 (1980).

2.  W. Fawcett and P. C. Herbert, J. Phys. C1, 1641 (1974).

3.  R. E. Hayes and R. M. Raymond, Appl. Phys. Lett. 31, 300 (1977).

4.  R. L. Bell, Negative Electron Affinity Devices (Clarendon Press, Oxford, 1973).

5.  R. E. Simon and W. E. Spicer, Phys. Rev. 119, 621 (1960).

6.  R. E. Simon and W. E. Spicer, J. Appl. Phys. 31, 1505 (1960).

7.  R. L. Bell, L. W. James and R. L. Moon, Appl. Phys. Lett. 25, 645.

8.  J. S. Escher, R. L. Bell, P. E. Gregory, S. B. Hyder, T. J. Maloney and G. A. Antypas, IEEE Trans Electron Devices ED-27, 1244 (1980).

9.  J. S. Escher, R. D. Fairman, G. A. Antypas, R. Sankaran, L. W. James and R. L. Bell, CRC Crit. Rev. Solid State Sci. 5, 577 (1975).

10. J. S. Escher, P. E. Gregory, G. A. Antypas, R. Sankaran and Y. M. Houng, J. Appl. Phys. 49, 447 (1978).

11. J. S. Escher, P. E. Gregory, S. B. Hyder and R. Sankaran, J. Appl. Phys. 49, 2591 (1978).

12. J. S. Escher, P. E. Gregory, S. B. Hyder, R. R. Saxena and R. L. Bell, IEEE Electron Device Lett. EDL-2, 123 (1981).

13. Final Tech. Report on Contract DAAK02-74-C-0132 (June 1980).

14. Final Tech. Report on Contract DAAG29-76-C-0002 (September 1978).

15. P. E. Gregory, J. S. Escher, S. B. Hyder, Y. M. Houng and G. A. Antypas, J. Vac. Sci. Technol. $\underline{15}$, 1483 (1978).

16. R. L. Moon, G. A. Antypas and L. W. James, J. Electron. Matls. $\underline{3}$, 635 (1974).

17. R. R. Saxena, S. B. Hyder, P. E. Gregory and J. S. Escher, J. Crys. Growth $\underline{50}$, 481 (1980).

18. S. B. Hyder, R. R. Saxena, S. H. Chiao and R. E. Yeats, Appl. Phys. Lett. $\underline{35}$, 787 (1978).

19. G. H. Olsen, J. Crys. Growth $\underline{31}$, 223 (1975).

20. C. L. Anderson and C. R. Crowell, Phys. Rev. $\underline{B5}$, 2267 (1972).

21. J. W. Matthews and A. E. Blakeslee, J. Crys. Growth $\underline{27}$, 118 (1974).

22. J. W. Matthews, A. E. Blakeslee and S. Mader, Thin Solid Films $\underline{33}$, 253 (1976).

23. J. W. Matthews and A. E. Blakeslee, J. Vac. Sci. Technol. $\underline{14}$, 989 (1977).

24. A. C. Gossard, P. M. Petroff, W. Wiegmann, R. Dingle and A. Savage, Appl. Phys. Lett. $\underline{29}$, 323 (1979).

25. P. E. Luscher, Solid State Technol. $\underline{20}$, 43 (1977).

26.  M. Ettenberg, C. J. Nuese, J. R. Appert, J. J. Gannon and R. E. Enstrom, J. Electron. Matls. $\underline{4}$, 37 (1975).

27.  N. Susa, Y. Yamauchi, H. Ando and H. Kanbe, Jap. J. Appl. Phys. $\underline{19}$, 117 (1979).

28.  R. Sankaran, R. L. Moon and G. A. Antypas, J. Crys. Growth $\underline{33}$, 271 (1976).

29.  S. B. Hyder, Proc. NATO-sponsored InP Workshop, June 1980, Hanscom AFB, MA, publication RADC-TM-80-07 and J. Crys. Growth, to be published.

30.  T. J. Maloney, M. G. Burt, J. S. Escher, P. E. Gregory, S. B. Hyder and G. A. Antypas, J. Appl. Phys. $\underline{51}$, 2879 (1980).

31.  F. G. Derbenwick, D. T. Pierce and W. E. Spicer, Methods of Experimental Physics, Vol. III, Solid State Physics, ed. by R. V. Coleman (Academic Press, New York, 1974), p. 67.

32.  F. G. Allen and G. W. Gobeli, Phys. Rev. $\underline{144}$, 558 (1966).

33.  T. H. DiStefano and D. T. Pierce, Rev. Sci. Instrum. $\underline{41}$, 180 (1970).

# VIII. PUBLICATIONS

The following papers were published under work sponsored all or in part by this contract.

1.  G. A. Antypas, Y. M. Houng, R. L. Moon, S. B. Hyder, J. S. Escher and P. E. Gregory, "Gallium Incorporation in LPE In$_{.53}$Ga$_{.47}$As Growth on (100) and (111)B InP Substrates at 600-650°C" in Gallium Arsenide and Related Compounds, 1978, Conf. Ser. 45, C. M. Wolfe, ed., (Institute of Physics, London, 1979), p. 89.

2.  P. E. Gregory, J. S. Escher, R. R. Saxena and S. B. Hyder, "Field-Assisted Photoemission to 2.1 Microns from a Ag/p-In$_{0.77}$Ga$_{0.23}$As Photocathode," Appl. Phys. Lett. 36, 639 (1980).

3.  T. J. Maloney, M. G. Burt, J. S. Escher, P. E. Gregory, S. B. Hyder and G. A. Antypas, "Quantum Efficiency of InP Field-Assisted Photo-cathodes," J. Appl. Phys. 51, 2879 (1980).

4.  J. S. Escher, R. L. Bell, P. E. Gregory, S. B. Hyder, T. J. Maloney and G. A. Antypas, "Field-Assisted Semiconductor Photoemitters for the 1-2 µm Range," IEEE Trans. ED-27, 1244 (1980).

5.  R. R. Saxena, S. B. Hyder, P. E. Gregory and J. S. Escher, "Vapor Phase Epitaxial Growth of InGaAs/InAsP Heterojunctions for Long Wavelength Transferred Electron Photocathodes," J. Crys. Growth 50, 481 (1980).

6.  J. S. Escher, P. E. Gregory, S. B. Hyder, R. R. Saxena and R. L. Bell, "Photoelectric Imaging in the 0.9-1.6 Micron Range," Electron Device Lett. EDL-20, 123 (1981).

7.  Y. G. Chai and R. Chow, "MBE Growth of Lattice-Mismatched In$_{0.77}$Ga$_{0.23}$As on InP," submitted to Appl. Phys. Lett.

DA
FIL